Disorder- and magnetic field–tuned fermionic superconductor-insulator transition in MoN thin films: Transport and scanning tunneling microscopy

M. Kuzmiak,[1,2] M. Kopčík,[1,2] F. Košuth,[1,3] V. Vaňo,[1,2] J. Haniš,[1,3] T. Samuely [ORCID],[3] V. Latyshev [ORCID],[3] O. Onufriienko,[1]
V. Komanický,[3] J. Kačmarčík [ORCID],[1] M. Žemlička,[4] M. Gmitra,[1] P. Szabó [ORCID],[1,*] and P. Samuely[1]

[1]*Centre of Low Temperature Physics, Institute of Experimental Physics, Slovak Academy of Sciences, SK-04001 Košice, Slovakia*
[2]*Department of Physics, Faculty of Electrical Engineering and Informatics, Technical University of Košice, SK-04001 Košice, Slovakia*
[3]*Institute of Physics, Faculty of Science, Pavol Jozef Šafárik University in Košice, SK-04001 Košice, Slovakia*
[4]*QphoX B.V., Elektronicaweg 10, 2628XG Delft, Netherlands*

Superconductor-insulator transition (SIT) driven by disorder and transverse magnetic field has been investigated in ultrathin MoN films by means of transport measurements and scanning tunneling microscopy and spectroscopy. Upon decreasing thickness, the homogeneously disordered films show increasing sheet resistance R_s, shift of the superconducting transition T_c to lower temperatures with the 3-nm MoN being the last superconducting film and thinner films already insulating. Fermionic scenario of SIT is evidenced by applicability of the Finkel'stein's model, by the fact that T_c and the superconducting gap Δ are coupled with a constant ratio, and by the spatial homogeneity of the superconducting and electronic characteristics. The logarithmic anomaly found in the tunneling spectra of the nonsuperconducting films is further enhanced in increased magnetic field due to the Zeeman spin effects driving the system deeper into the insulating state and pointing also to fermionic SIT.

I. INTRODUCTION

A quantum phase transition from superconducting to insulating state (SIT) can be induced in quasi-two-dimensional systems by disorder or magnetic field. This transition occurs at the critical disorder, where the electron's mean free path is extremely small and the Ioffe-Regel parameter, the product of the Fermi momentum and the mean free path $k_F l$ is close to unity [1,2]. We distinguish two SIT mechanisms depending on whether the growing disorder affects the amplitude or the phase of the superconducting wave function [2]. At the loss of long-range phase coherence superconducting condensate melts into locally coherent superconducting islands which can survive even in the insulating state [3]. This is termed a bosonic SIT. A fermionic SIT occurs when disorder reduces the electronic screening of the Coulomb interaction and the amplitude of the wave function is suppressed. Then, transition temperature T_c and superconducting order parameter/gap Δ disappear at once and a bad metallic phase is formed before a transition to the insulating state at even higher disorder [4].

The bosonic SIT has been observed by scanning tunneling spectroscopy in TiN, InO$_x$, NbN and a-MoGe showing emergence of local superconducting puddles with varying superconducting gap present on both superconducting and insulating sides of the transition and a pseudogap above critical temperature T_c or magnetic field B_{c2} [5–11]. Loss of phase coherence can also be manifested by variation of the coherence peaks height of the superconducting tunneling spectra among individual puddles [9,12,13]. Recent scanning tunneling microscopy (STM) experiments of Dutta *et al.* [14] performed

on ultrathin a-MoGe films near critical disorder show a Bose (bad) metallic state above the critical field still revealing traces of superconducting gap. Then, in both scenarios quantum transition from superconducting to bad metallic state may happen before the insulating state is achieved.

At fermionic SIT when increased Coulomb interaction is operative, neither pseudogap above T_c or B_{c2}, nor spatial variation of the superconducting gap appear, i.e., "fermionic" systems are spatially homogeneous at homogeneous disorder. Recently, Carbillet *et al.* [15,16] showed that inhomogeneities of the gap on the scale much larger than the superconducting coherence length ξ can appear in the fermionic SIT as well. This is due to emerging inhomogeneities of the normal state where the strength of the Altshuler-Aronov effect varies. Early tunneling experiments performed on planar tunnel junctions suggested a fermionic mechanism for the SIT in Bi and PbBi/Ge thin films [17,18]. In our works on disordered ultrathin MoC films [19,20] we presented direct evidence that T_c and Δ are simultaneously suppressed and superconductivity remains spatially homogeneous very close to SIT. When SIT was driven by magnetic field oriented perpendicularly to the heavily disordered but still superconducting MoC film, surprisingly, the Zeeman paramagnetic effects dominated over orbital coupling on both sides of the transition [20].

Here, we present studies on MoN films starting from 30-nm thickness down through the whole SIT where 3-nm MoN is the last superconducting film and thinner films no longer exhibit superconductivity on large scale as evidenced by resistive measurements. Based on our transport and low-temperature STM measurements we show that the SIT in MoN thin films tuned by both disorder and/or magnetic fields is realized by the fermionic pathway. In particular, the spin-dependent Altshuler-Aronov (AA) effect in insulating state

*Corresponding author: pszabo@saske.sk

184511-1

points to the dominance of Zeeman effects supporting the fermionic scenario.

II. EXPERIMENTAL

Molybdenum forms several nitrides including cubic γ-phase of Mo_2N, tetragonal β-Mo_2N and hexagonal δ-MoN [21]. The γ phase has a superconducting transition at about 5 K [22,23]. Recently, Tsuneoka *et al.* [24] prepared series of thin γ phase Mo_2N films down to 1.5-nm thickness showing the SIT. Here, we have prepared the high quality Mo_2N thin films with $t = 30$-, 10-, 5-, 3-, 2-, 1.5-nm thicknesses by reactive magnetron sputtering onto a sapphire substrate from a Mo target in an argon-nitrogen mixture gas atmosphere. The crystal structure of the films was characterized by x-ray diffraction. Our films reveal a face-centered-cubic crystalline structure, which is typical for a $\gamma-Mo_2N$ phase [25,26].

The basic characterization of our samples was done by transport measurements. A more detailed discussion can be found in the Supplemental Material [27], where the determination of the Ioffe-Regel parameter [1] is explained and the analysis of our data in terms of the Finkel'stein's model [4] is also described. We applied STM measurements to study the quasiparticle density of states (DOS) of our samples. The experiments were performed in a homemade STM system immersed in a Janis SSV ^{3}He cryostat, which allows measurements down to $T = 0.3$ K in magnetic fields up to $B = 8$ T. A gold STM tip was used to measure the *ex situ* prepared samples. At each point of the sample surface, first a topography was acquired with the feedback loop on, then the feedback loop was turned off and the tunneling current was recorded while sweeping the bias voltage, all on the grid of 128×128 topography points.

The tunneling conductance was calculated by numerical differentiation of the *I-V* curves. The *dI(V)/dV* spectra measured through the tunnel junction between a normal metal and a superconductor can be described by the equation

$$\frac{dI(V)}{dV} = N \int_{-\infty}^{\infty} N_S(E) \left[\frac{-\partial f(E + eV)}{\partial eV} \right] dE, \quad (1)$$

where $E = eV$ is the energy and the derivative of the Fermi distribution in the square brackets represents thermal smearing. N is the constant DOS of the metallic tip, and N_S represents the superconducting DOS, respectively. The BCS theory defines N_S as

$$N_S(E) = \text{Re}\left(\frac{E}{\sqrt{E^2 - \Delta^2}} \right), \quad (2)$$

where Δ is the superconducting energy gap. Tunneling spectra with spectral smearing higher than the thermal broadening can be described by the phenomenological modification of the Bardeen-Cooper-Schrieffer (BCS) DOS of Dynes [28] who introduced a complex energy $E = E'-i\Gamma$, where Γ is the spectral smearing parameter. The nonzero value of this parameter can be connected with pair-breaking centers at the tunnel junction area [29]. If the superconductor is in the normal state and $\Delta = 0$, the DOS will be constant in the case of standard metals. However, in the case of highly disordered metals, we must account for corrections related to the enhanced electron-electron interaction. According to the AA theory of

two-dimensional (2D) systems [30,31] this is manifested by a logarithmic reduction of the normal state DOS at Fermi energy down to the thermal energy defined by the measuring temperature. The standard AA correction is not a function of the applied magnetic field. However, when the electron spins are taken into account in the particle-hole channel the AA correction to the normalized DOS $N_N(E) = 1 - \delta N$ reveals field dependence, described as [31]

$$\delta N(E, T, B) \approx A \left\{ f(E, \Gamma_0) + \frac{\lambda_1}{2\lambda_0} \left[f(E, \Gamma_0) \right. \right.$$
$$\left. \left. + \frac{1}{2} \sum_{\alpha=\pm 1} f(E + \alpha E_Z, \Gamma_0) \right] \right\}, \quad (3)$$

where A includes all constants and parameters of the tunneling barrier, f is the logarithmic function defined in [20] with arguments normalized to the thermal energy and $E_Z = 2 \mu_B B$ is the Zeeman energy, with μ_B being the Bohr magneton and B magnetic field. The constants of λ_0 and λ_1 describe the interaction of an electron and a hole with total spin 0 and 1, respectively and Γ_0 is responsible for the broadening of the AA logarithmic singularity [20]. The first and the second terms originate from the interaction of the electron and the hole with a zero projection of the total spin on the direction of the magnetic field, and the third (and fourth) term from interactions with opposite spins. In the case when the ratio $\lambda_1/2\lambda_0$ is from interval $\langle -1/3, 0 \rangle$ at zero magnetic field the logarithmic anomaly of the first term is partly compensated by three equal logarithmic terms with opposite sign. In the presence of applied magnetic field a part of the electronic DOS at the Fermi energy is removed due to spin polarization and two singularities/maxima should appear at $E = \pm E_Z$. Then, the logarithmic singularity/minimum at the Fermi level is more pronounced than it was in the zero-field case.

III. RESULTS

The temperature dependences of the sheet resistance $R_s(T)$ obtained on 30-, 10-, 5-, 3-, 2-, and 1.5-nm thin MoN films at temperatures from 100 down to 0.3 K are shown in Fig. 1(a). The thickest 30-nm sample shows an almost temperature independent sheet resistance down to the superconducting transition at $T_c = 5.83$K. With reducing film thickness the normal state sheet resistance R_s increases, the derivative dR_s/dT becomes negative and a gradual shift of the superconducting transition typical for homogenously disordered systems is visible down to $T_c = 2.8$K in the case of the 3-nm sample. The evolution of this disorder-tuned superconductor-insulator transition can be followed in Fig. 1(b), where the critical temperature T_c (blue symbols-left scale) and the Ioffe-Regel parameter $k_F l$ (green symbols-right scale) are shown as the function of the film thickness. The inset of Fig. 1(b) shows T_c as a function of the sheet resistance R_s by open black symbols. The solid red line is the fit to the Finkel'stein's formula [4] with the fitting parameters of the critical resistance $R_{cr} = 2.3$ kΩ where the superconductivity terminates, the critical temperature of the bulk phase $T_{c0} = 6.34$K and the elastic scattering time $\tau = 2.66 \times 10^{-16}$ s. The rapid decrease of the $k_F l$ values with reducing film thickness and the low
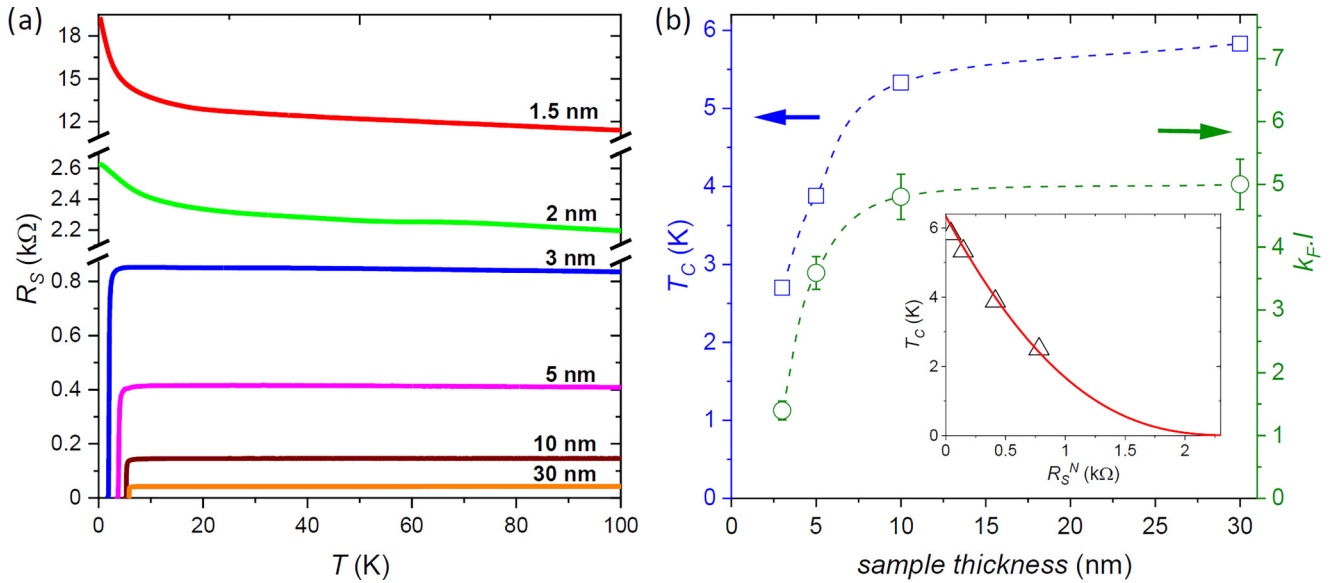
FIG. 1. (a) Evolution of the temperature dependences of the sheet resistance $R_S(T)$ with various thicknesses of MoN thin films. Film thicknesses are shown above the respective curves. (b) The main panel shows thickness dependences of the critical temperature T_C (blue color, symbol) and the Ioffe-Regel parameter $k_F l$ (green color, symbol ◯). The T_C values have been determined at 50% of the normal state sheet resistance. The inset shows the dependence of the normal state sheet resistance R_S^N on the critical temperature T_C (black △ symbols). The red curve is a fit to the Finkel'stein's model with fitting parameters given in the legend. The analysis of the transport data is described in detail in the Supplemental Material [27].

value of $k_F l \sim 1.4$ determined at the 3-nm sample suggest that this superconducting sample is in the near proximity to critical disorder. From transport measurements in transverse magnetic field the upper critical magnetic field was also determined, see Fig. S1 and S2 in Supplemental Material [27].

Low temperature STM measurements were performed to study the surface topography of our thin films. Figure S3 presented in the Supplemental Material [27] shows typical topography images of the MoN thin films from both sides of the SIT. The samples had clean surfaces with continuous and compact polycrystalline structure. The images shown in Fig. S3 [27] can be characterized by the average surface corrugations $\sim 1.2-$, 0.5-, and 0.35-nm for the 30-, 3-, and 2-nm samples, respectively. The sharp, well defined grain boundaries and the low averaged surface corrugations point to high quality of the studied thin films.

In Fig. 2, representative temperature dependences of the STM tunneling spectra measured on 30-, 3-, and 2-nm samples are shown in Figs. 2(a), 2(b), and 2(c), respectively. The upper panels show 3D plots of the zero-field temperature dependences of the $dI(V)/dV$ spectra. The spectra taken on 30- and 3-nm samples reveal standard superconducting features. At increased temperature the superconducting gap structure bordered by symmetrical coherence peaks is suppressed at T_c and at higher temperatures constant normal state tunneling spectra are visible. The value of the superconducting energy gap Δ and its temperature dependence in both sets of the samples have been determined from fitting to Dynes modification of the BCS DOS. The fitting curves (open symbols) and experimental data (lines) at the indicated temperatures are shown in the corresponding lower panels. We can see clearly that the model describes the experimental data perfectly. The obtained temperature dependences of

the energy gap are shown in Fig. S4 of the Supplemental Material [27]. The gap values reveal BCS-like temperature dependences with $\Delta(0) = 0.87$ meV, $\Gamma/\Delta \sim 0.06$ meV, $T_c = 5.6$ K, $2\Delta(0)/k_B T_c \sim 3.6$ for 30-nm and $\Delta(0) = 0.44$ meV, $\Gamma/\Delta \sim 0.4$ meV, $T_c = 2.9$ K, $2\Delta(0)/k_B T_c \sim 3.55$ for the 3-nm sample. Figure 2(c) shows the effect of temperature on the tunneling spectrum measured on the nonsuperconducting 2-nm film. No coherence peaks indicative of superconductivity are observed at the lowest temperature $T = 0.5$ K but the spectrum reveals a logarithmiclike reduction towards zero-bias voltage. We fit our experimental data to the thermally smeared AA correction, defined in Eq. (3). The curve taken at the lowest temperature is fit by parameters: $A = -0.26$, $\lambda_1/2\lambda_0 = -0.12$, $\Gamma_0 = 0.15$ meV and $B = 0$ T. In the fits at higher temperatures, only the temperature was changed and the smearing parameter varied slightly in the range of 5%. The agreement between our data (lines) and the thermally smeared AA correction (symbols) fit indicates, that what we observe is not the temperature dependence of the logarithmic reduction, but only the effect of increased thermal smearing with energy $\sim k_B T$.

We also studied the effect of perpendicular magnetic field on the tunneling spectra on samples with thicknesses of 30-nm, 3-nm, 2-nm and 1.5-nm at $T = 0.5$ K. The magnetic dependence of the $dI(V)/dV$ spectra measured on the thickest 30-nm superconducting sample shown in Fig. S5 in the Supplemental Material [27] reveals a classical behavior. In increasing field, the position of gaplike peaks shifts to lower voltage and the gap gradually closes. This process can be better followed in the side view shown in the inset of Fig. S5 and in top view of Fig. S6a) in the Supplemental Material [27]. The upper critical magnetic field of the 30-nm sample is above the range of our experimental setup (Fig. S2
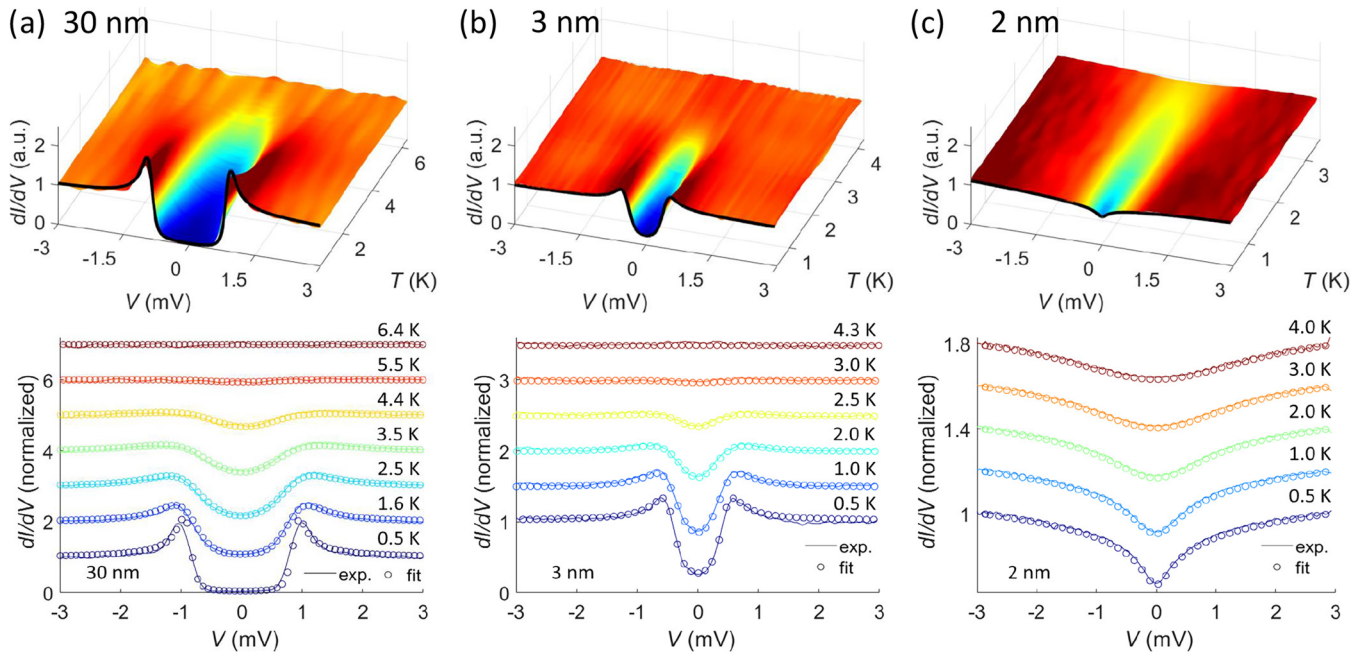
FIG. 2. Color plots of the typical STM tunneling spectra measured on MoN thin films with 30-, 3-, and 2–nm thicknesses at different temperatures at $B = 0$ T. (a), (b), (c) are shown in the upper panels. All spectra have been normalized to their values at 3 mV bias. The tunneling spectra from (a) and (b) were fitted to Dynes formula, spectra from (c) to Altshuler-Aronov effect defined in formula (1) including thermal smearing in all cases. Selected experimental curves from the upper panels (lines) and the fitting curves (symbols) are shown in the corresponding lower panels.

in the Supplemental Material [27]), so we could not detect a full transition to the normal state.

The main panels at the top of Fig. 3 show 3D plots of the effect of perpendicular magnetic field on the tunneling spectra on the 3-, 2-, and 1.5-nm thin films. The insets show side views of the corresponding magnetic dependences. Figure 3(a) plots the effect of magnetic field on the thinnest (3-nm) superconducting sample that is close to the critical disorder. Again, at increasing field the gap peaks are getting more smeared and the in-gap area is gradually filled but remarkably, the gap-peak position remains unchanged and before the conductance $dI(V)/dV$ gets completely flat at the upper critical magnetic field $B_{c2} \sim 5$ T, the "gap" structure holds and is even enhanced in further increased field. The both effects are also documented in Fig. S6 b) of Supplemental Material [27]). We have seen similar effects of the magnetic field on ultrathin MoC films in our previous paper [20], where we studied the magnetic field induced SIT in these samples. The both unusual features were described by the Zeeman effect on the density of states, namely, the constant position of the gap peak as due to spectral broadening of the Zeeman split superconducting gap peaks and enhanced gap in the normal state due to Zeeman effect on spin dependent AA correction to DOS. There, based on the work of [29], to describe the total DOS we used the product of $N(E) = N_S^D(E)N_N(\Omega)$, where N_S^D is the Dynes modification of the BCS DOS (2) with smearing parameter Γ, $N_N(\Omega)$ represents spin dependent AA corrections defined in (3), and the energy-dependent parameter $\Omega(E) = \mathrm{Re}[\sqrt{(E + i\Gamma)^2 - \Delta^2}]$ ensures the balance of quasiparticles after the transition to the superconducting state. Here, we employ this model to describe the magnetic field dependence of the tunneling spectra measured on our

3-nm thin MoN superconducting sample. We started to fit our spectra in the normal state at $B = 8$ T without superconducting contribution. We determined the values of the parameters $A = -0.3$, $\lambda_1/2\lambda_0 = -0.24$, $\Gamma_0 = 0.31$ meV which we used to fit the complete magnetic dependence down to $B = 0$ T. During the fit in the superconducting state at $B < B_{c2}$ we used only the value of the energy gap as a fit parameter, which we varied according to formula $\Delta = \Delta(0)\sqrt{1 - B/B_{c2}}$, in agreement with our results on MoC [20]. The bottom panel of Fig. 3(a) shows the results of our fit (open symbols) together with selected experimental curves from the upper panel (solid lines). The magnetic field dependence of the AA correction used during the fit is shown in Fig. S7 of the Supplemental Material [27]. It can be seen that the small AA correction at $B = 0$ T with the ZBC value of ~ 0.95 is enhanced by $\sim 20\%$ to the value of ~ 0.75 at $B = 8$ T.

While in the 3-nm MoN film and similarly in MoC films in our previous study [20] superconductivity and AA effect interfere, in the thinner MoN samples one can focus on the AA effects only. As can be seen in Figs. 3(b) and 3(c) the AA effect (reduction of the DOS at Fermi energy) gets stronger on the thinner and more disordered 1.5-nm sample compared to 2-nm MoN film. Most importantly, also the amplifying effect of magnetic field on the AA reduction is unambiguously detected, here: the zero-bias conductance drops by roughly $\sim 10\%$ from ~ 0.67 on 2-nm film and $\sim 4\%$ from 0.52 for the 1.5-nm film when the magnetic field is increased from $B = 0$ to 8 T.

To describe these magnetic field dependences quantitatively, we fit the spectra at selected magnetic fields as shown in the lower panels of Figs. 3(b) and 3(c). Since these samples are not superconducting, the superconducting contribution
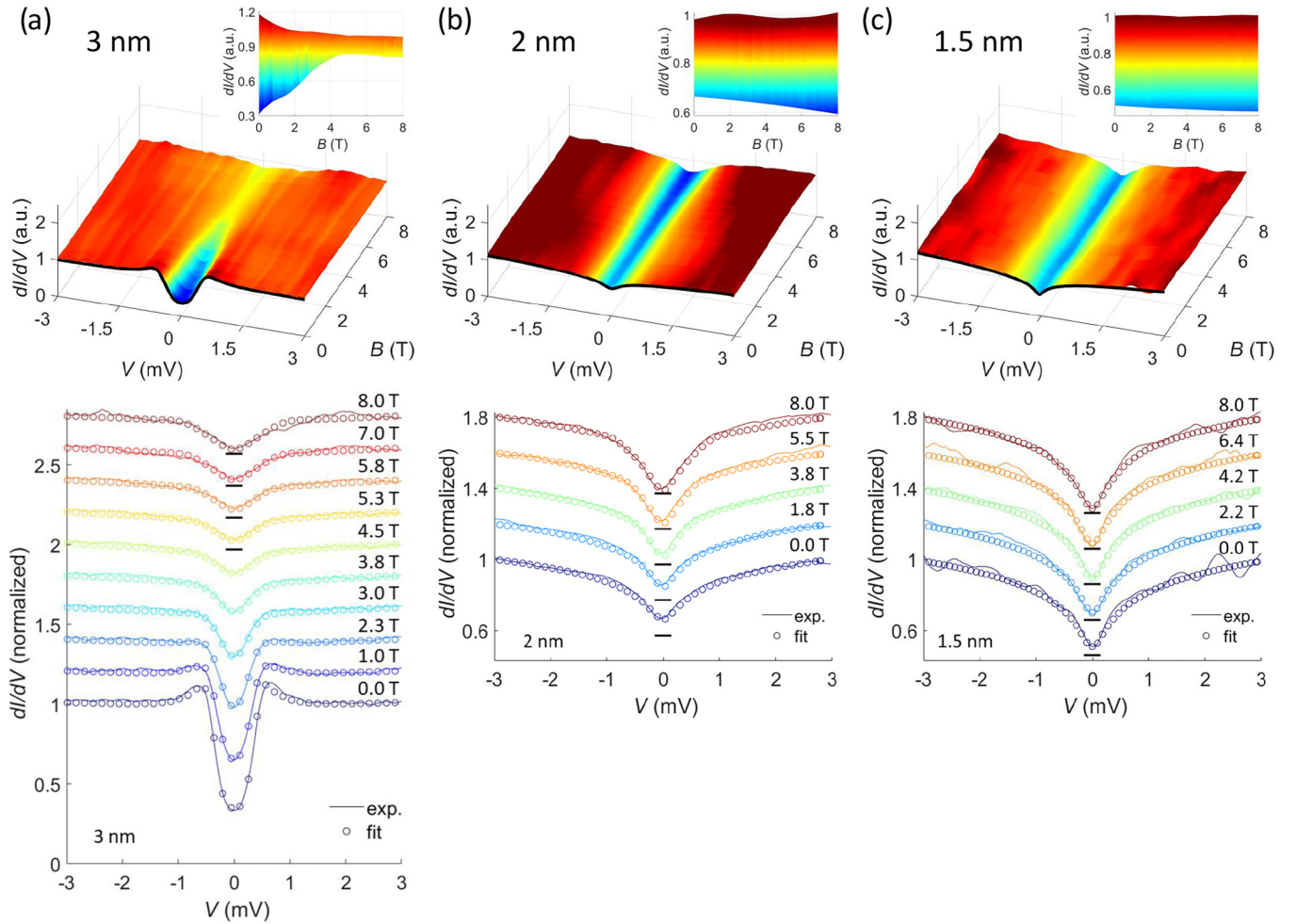
FIG. 3. Color plots of the typical STM tunneling spectra measured on MoN thin films with 3-, 2-, and 1.5–nm thicknesses at different magnetic fields at $T = 0.5$ K. (a), (b), (c) are shown in the upper panels. All spectra have been normalized to their values at 3-mV bias energy. The magnetic field dependences from (a) and (b) correspond to spectra shown in Figs. 2(b) and 2(c). The tunneling spectra from (a) were fitted to Dynes formula including Altshuler-Aronov corrections, spectra from (b) and (c) to Altshuler-Aronov effect defined in formula (3) including thermal smearing in both cases. Selected experimental curves from the upper panels (lines) and the fitting curves (symbols) are shown in the corresponding lower panels. The horizontal black lines at each set are positioned to the conductance values (at $B = 8$ T) 0.75, 0.6 and 0.48 for 3-, 2-, and 1.5-nm thin films, respectively.

from the total density of states falls out, and we can fit the tunnel spectra to the DOS defined as $N_N(E) = 1 - \delta N$ according to formula (3). We started to fit the spectra again at the highest field $B = 8$ T, where we obtained the following fitting parameters: $A = -0.26$, $\lambda_1/2\lambda_0 = -0.12$, $\Gamma_0 = 0.17$ meV for the 2-nm sample and $A = -0.23$, $\lambda_1/2\lambda_0 = -0.035$, $\Gamma_0 = 0.14$ meV for the 1.5-nm sample. At lower magnetic fields only the value of Γ_0 was slightly corrected by less then 3%.

As a result, the spin dependent AA correction to the normal density of states describes well the effect of magnetic field in the both nonsuperconducting samples, and also in our thinnest 3-nm superconducting sample. In the latter case remarkably, the field dependent AA correction contributes very weakly ($< 4\%$) to the total DOS in the superconducting state at $B < B_{c2}$ (Fig. S7 in the Supplemental Material [27]).

In Fig. 4, we compare the AA effect in zero magnetic field in 3-, 2-, and 1.5-nm samples. In the case of the 3-nm sample, we plot only the fitting curve of the contribution of the AA

effect because in the experiment the total DOS comprises also the superconducting part. One can see a rapid enhancement of the AA correction upon decreasing the thickness/increasing disorder which is even amplified by the fact that spin dependent contributions partly compensating the leading AA term are also diminished with disorder.

IV. DISCUSSION

In the following we argue that the SIT introduced in our thin MoN films by disorder and magnetic field follows the fermionic scenario.

The first argument is based on the fact that superconducting transition temperature T_c versus the films sheet resistance R_s in Fig. 1 follows the predictions of the Finkel'stein's model based on enhanced Coulomb effects leading to suppression of the amplitude of the order parameter and T_c at once [4]. This finding has also been documented in our transport measurements on strongly disordered MoC films [19] and in other
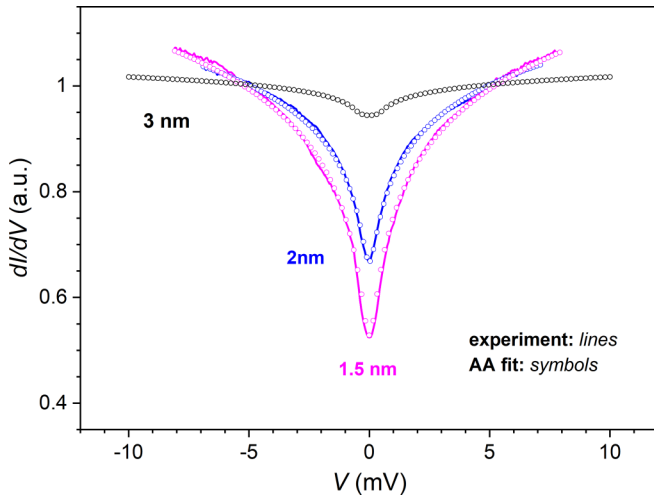
FIG. 4. Typical tunneling spectra measured in the nonsuperconducting samples with 1.5- and 2-nm thicknesses (pink and blue line, respectively) at $T = 0.5$ K. The fitting curves to Altshuler-Aronov model are shown with symbols of corresponding color. The black symbols show the theoretically calculated Altshuler-Aronov contribution to the total DOS at the superconducting 3–nm sample at $B = 0$ T. All curves were normalized to their 5 mV bias values.
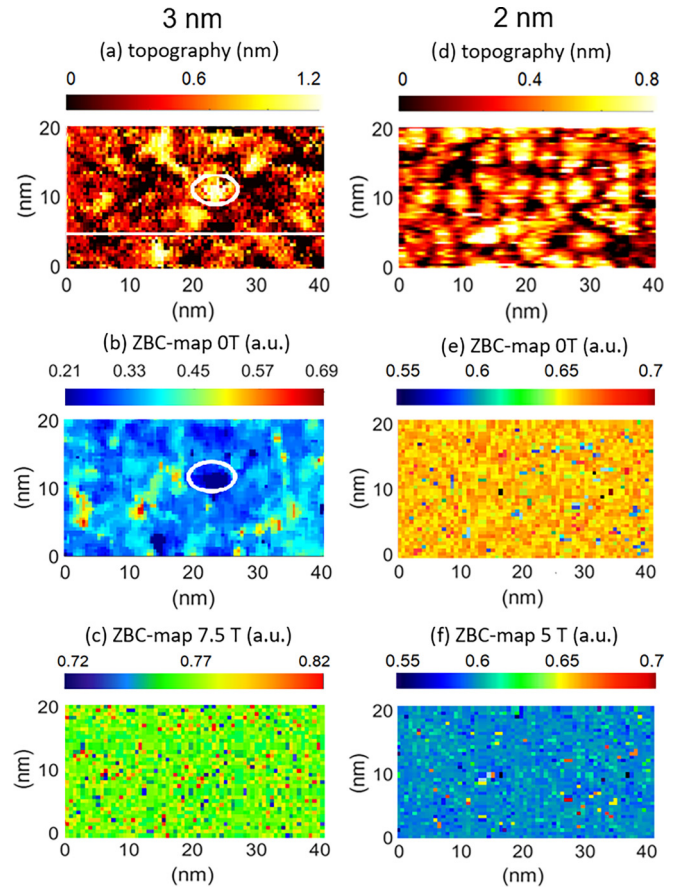

FIG. 5. Surface topographies (a), (d) and the corresponding Zero-Bias-Conductance (ZBC) maps (b), (c), (e), (f) of the superconducting 3-nm (left panels) and nonsuperconducting 2-nm (right panels) MoN thin films taken at indicated magnetic fields. 3-nm-nm sample shows protrusions as this in the oval in (a) which is reflected also in deeper ZBC data in the oval in (b) taken in superonducting state at $T = 0.5$ K and $B = 0$ T while above B_{c2} this contrast is lost, see (c). Protrusions found in fully nonsuperconducting 2-nm-nm sample in (d) has no reflections in either of ZBC maps in (e) and (f).

materials as for example MoGe films [32]. Tsuneoka *et al.* [24] who prepared a series of MoN films from 60-nm down to 1.5-nm with T_c decreasing from 6.6 down to 2.5 K and the SIT transition at about 5-nm thin films also argued that T_c depression obeys the fermionic scenario according to the amplitude fluctuation in the order parameter. They could fit T_c as a function of the sheet resistance to the Finkel'stein's model with the following parameters: the bulk $T_{c0} = 6.45$ K, the critical resistance $R_{\rm cr} = 2\,{\rm k\Omega}$ and the elastic scattering time $\tau = 1.6 \times 10^{-16}$ s values very close to ours. It should be noted that the suppression of T_c with increasing value of R_s has also been observed in systems with an evident bosonic SIT, hence the validity of the Finkelstein model is a necessary but not a sufficient condition of the fermionic model [11].

The second evidence supporting the fermionic SIT is based on the fact that with increasing disorder the superconducting energy gap Δ and the transition temperature are suppressed simultaneously and the superconducting coupling is constant, not depending on the increasing disorder. In our case it is so and the coupling parameter is $2\Delta(0)/k_B T_c \sim 3.5$–3.6 for the 30-nm film down to 3-nm MoN (see Fig. S4 in [27]). This has also been observed in our previous paper in MoC films [19].

The third argument employs the fact that spectral characteristics on increasingly disordered superconductors remains homogeneous, i.e., a long-range coherence holds and no local variations of the superconducting gap emerge. We have studied the superconducting energy gap locally by the STM measurements on all our superconducting samples down to 3-nm thickness close to the critical disorder. The gap maps constructed from these measurements, as well as the zero-bias conductance maps (ZBC) demonstrate the homogeneity of the superconducting state on the flat regions of the investigated surfaces. Homogeneity of tunneling spectra measured on the 3-nm sample along a 40-nm white line from Fig. 5(a) is presented in the form of top view on spectra in Fig. 6(a).

We also studied the coherence-peaks height map on the 3-nm sample, which could reflect the loss of phase coherence, too [9,12,13]. Before constructing this map, we normalized all tunneling spectra to the contribution of the AA effect at $B = 0$ T (black symbols in Fig. 4) determined from fit in Fig. 3. In contrast to experiment on NbN [9] we could not find any distinct variations in the coherence peak heights. On the other hand, we admit that with the high spectral smearing with $\Gamma/\Delta \sim 0.4$ it would be difficult.

In some areas of the 3-nm thin superconducting film, islands a few nanometers wide with slightly different values of the superconducting energy gap than in other locations are observed. However, as already shown in our previous paper [33] such a variation occurs at the places with slightly more pronounced protrusions/thicknesses of the film and a good correlation exists between the topography and the gap maps. The thicker the area the bigger the energy gap Δ and the smaller the spectral smearing Γ. As we have already shown on MoC disordered films [34] the effect is connected with the
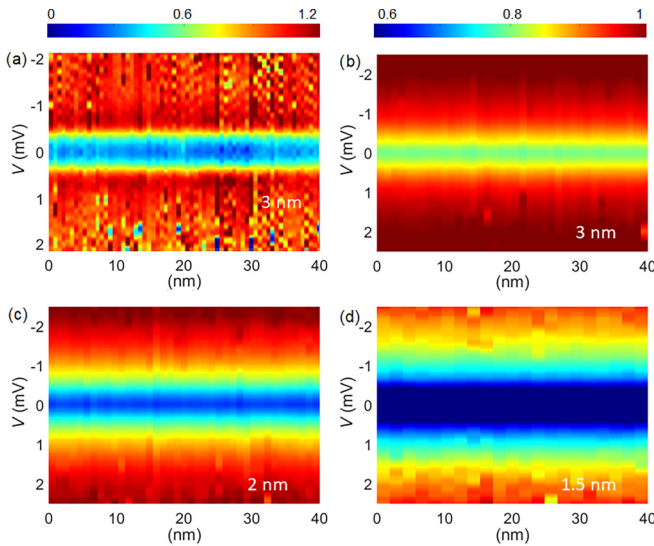
FIG. 6. Typical 40-nm-nm long linecuts of the tunneling spectra constructed from the spectral maps measured on 3-nm-nm thin film in the superconducting ($T = 0.5$ K and $B = 0$ T) and normal state ($B = 7.5$ T $> B_{c2}$) in (a) and (b), respectively, and on nonsuperconducting 2-nm and 1.5-nm thin films ($T = 0.5$ K and $B = 0$ T), (c) and (d), respectively. Tunneling spectra in (a) are taken along the white line in Fig. 5(a). (b)–d) are plotted in the same color scale, shown above (b).

pair-breaking fields at the interface between the substrate and the thin film.

Obviously, the question may arise how close to SIT the disordered films would have to be for bosonic effects to occur, and whether our 3-nm MoN was that close. For example, in strongly disordered NbN [10] and α-MoGe [11] thin films, samples thicker than 8-nm and 5-nm, respectively, exhibit an evident fermionic scenario with a spatially homogeneous BCS-like gap, but on thinner samples with higher disorder, spatial inhomogeneities appear. Therefore, we study here for the first time not only strongly disordered superconducting samples near SIT but also nonsuperconducting MoN films that are already on the other side of the transition. Remarkably, the spectral maps taken on the 3-nm samples above B_{c2} and the spectral maps taken on the nonsuperconducting 2-nm and 1.5-nm samples measured at any field show no spatial variations regardless of any corrugations. While for the 3-nm MoN film in superconducting state the zero-bias conductance map taken at zero field in Fig. 5(b) reveals small variations in agreement with the topography in Fig. 5(a) (see for example the spots in the white ovals, where an increase of about 1-nm in the topography corresponds to a 30–50% lower ZBC due to locally bigger superconducting gap), on the contrary, the ZBC map in (c) taken at 7.5 T, i.e. above B_{c2}, features no areas correlated with topography, only noise with approx. 5% dispersion. In Fig. 5(d), the 2-nm MoN topography shows higher and lower spots, but no spatial changes are observed in the ZBC maps measured at 0 T and 5 T (see (e) and (f), respectively) except experimental noise. Similar ZBC maps without apparent spatial changes were also observed on the 1.5-nm sample. The 40-nm long linecuts, measured on the surfaces of the superconducting 3-nm thin film in the normal state above B_{c2} and nonsuperconducting 2-nm and 1.5-nm thin

films at $B = 0$ T shown in Figs. 6(b), 6(c), 6(d), respectively, also point to the homogeneity of the measured spectra.

Carbillet et al. [15,16] pointed out that inhomogeneities of the superconducting gap can appear due to local variations of the Altshuler-Aronov effect. They modeled the AA correction as $dI/dV \sim V^{\alpha}$ and showed the local variations in the α-maps on a rather long scale. We have also analyzed the spectral maps measured on 3-nm (at 7.5 T), 2-, and 1.5-nm MoN films at different fields on surfaces typically $50 \times 50-\text{nm}^2$ in a similar way but our α maps did not show any observable variations. However, we admit that it is not ruling out their existence completely, because of the small size of the studied surfaces and high spectral smearing of the MoN spectra.

Fourthly, we show, that the transverse magnetic field applied to the thin films in close proximity to SIT acts through paramagnetic Zeeman spin-splitting effect. In the previous work [20] on 3-nm superconducting MoC film paramagnetic Zeeman effects dominated on both sides of the field-tuned SIT. The critical magnetic field $B_{c2}(T)$ showed square root temperature dependence typical for paramagnetic pair breaking, the Zeeman effect was found in the superconducting density of states below B_{c2}, and at higher fields, in the normal state a depleted DOS due to AA effect was detected. Also, the logarithmic AA anomaly in DOS present in the STM spectra at B_{c2} was enhanced upon increasing magnetic field driving the system deeper into the insulating state. The MoN films close to SIT indicate very similar effects. The spin-dependent and spatially homogeneous AA effect on superconducting 3-nm and thinner nonsuperconducting samples is identified. Obviously this can be observed only in systems where the magnetic field acts on quasiparticles through Zeeman splitting. Therefore, it is very important that the magnetic field dependence of the superconducting energy gap $\Delta(B) \sim \sqrt{1 - B/B_{c2}}$ typical for the presence of paramagnetic pair breaking of Cooper pairs was necessary in the fits on the 3-nm superconducting sample. The temperature dependence of the critical magnetic field $B_{c2}(T)$ of our sample shown in Fig. S2 [27] also indicates the dominance of paramagnetic effects. This follows not only from the square-root curvature of $B_{c2}(T)$ in the vicinity of T_c (red dashed line) but also from the high value of $B_{c2}(0) \sim 4.5-5$ T close to the Clogston limit ($B^P[\text{T}] \simeq 1.8T_c[\text{K}]$) [35], which for the superconductor with $T_c = 2.9$K is $B^P = 5.2$ T. The determination of the B_{c2} values from our transport measurements is described in detail in the Supplemental Material [27]. Thus, in strongly disordered MoN thin films, when a transverse magnetic field is applied, Zeeman spin effects dominate both in the superconducting and the normal states.

The dominance of spin splitting effects has also been observed in systems that are close to the metal-insulator transition and exhibit "bad metallic" behavior due to strong electron correlations. Bogdanovich et al. [36] have shown that in boron-doped Si:B samples, the metal-insulator transition is controlled predominantly by electron correlations and orbital effects are unimportant despite strong spin-orbit effects.

V. CONCLUSIONS

MoN films reveal a transition from superconducting to insulating/bad metallic phase upon decreasing thickness from

30 to 1.5 nm. The superconducting transition temperature is gradually shifted from about 6 K to 2.7 K in the case of 3-nm films accompanied by decreasing Ioffe-Regel parameter approaching unity. Films thinner than 3 nm are already nonsuperconducting. The shift of T_c is also accompanied by the increase of the sheet resistance and can be modeled by the Finkel'stein's model for the enhanced electron interaction providing the critical sheet resistance $R_{cr} = 2.3 \, k\Omega$ where the superconductivity terminates. The STM and spectroscopy measurements prove that T_c and the superconducting gap Δ are coupled with a constant ratio for all films and that the superconducting DOS and the normal-state AA DOS corrections are spatially homogeneous and no emergent granularity appears on either sides of SIT. The logarithmic AA DOS correction, is enhanced in increased magnetic field due to

the Zeeman spin effects driving the system deeper into the insulating state. All this is pointing to purely fermionic SIT scenario in the system.

[1] A. F. Ioffe and A. R. Regel, Non-crystalline, amorphous and liquid electronic semiconductors, Prog. Semicond. **4**, 237 (1960).

[2] V. F. Gantmakher and V. T. Dolgopolov, Superconductor–insulator quantum phase transition, Phys.-Usp. **53**, 1 (2010).

[3] M. P. A. Fisher, Quantum phase transitions in disordered two-dimensional superconductors, Phys. Rev. Lett. **65**, 923 (1990).

[4] A. M. Finkel'stein, Superconducting transition temperature in amorphous films, Pisma Zh. Eksp. Teor. Fiz. **45**, 37 (1987) [Sov. Phys. JETP Lett. **45**, 46 (1987)].

[5] B. Sacépé, C. Chapelier, T. I. Baturina, V. M. Vinokur, M. R. Baklanov, and M. Sanquer, Disorder-induced inhomogeneities of the superconducting state close to the superconductor-insulator transition, Phys. Rev. Lett. **101**, 157006 (2008).

[6] B. Sacépé, C. Chapelier, T. I. Baturina, V. M. Vinokur, M. R. Baklanov, and M. Sanquer, Pseudogap in a thin film of a conventional superconductor, Nat. Commun. **1**, 140 (2010).

[7] B. Sacépé, T. Dubouchet, C. Chapelier, M. Sanquer, M. Ovadia, D. Shahar, M. Feigel'man, and L. Ioffe, Localization of preformed cooper pairs in disordered superconductors, Nat. Phys. **7**, 239 (2011).

[8] M. Chand, G. Saraswat, A. Kamlapure, M. Mondal, S. Kumar, J. Jesudasan, V. Bagwe, L. Benfatto, V. Tripathi, and P. Raychaudhuri, Phase diagram of the strongly disordered S-Wave superconductor NbN close to the metal-insulator transition, Phys. Rev. B **85**, 014508 (2012).

[9] A. Kamlapure, T. Das, S. C. Ganguli, J. B. Parmar, S. Bhattacharyya, and P. Raychaudhuri, Emergence of nanoscale inhomogeneity in the superconducting state of a homogeneously disordered conventional superconductor, Sci. Rep. **3**, 2979 (2013).

[10] Y. Noat, V. Cherkez, C. Brun, T. Cren, C. Carbillet, F. Debontridder, K. Ilin, M. Siegel, A. Semenov, H.-W. Hübers, and D. Roditchev, Unconventional superconductivity in ultrathin superconducting NbN films studied by scanning tunneling spectroscopy, Phys. Rev. B **88**, 014503 (2013).

[11] S. Mandal, S. Dutta, S. Basistha, I. Roy, J. Jesudasan, V. Bagwe, L. Benfatto, A. Thamizhavel, and P. Raychaudhuri, Destruction of superconductivity through phase fluctuations in ultrathin α-MoGe films, Phys. Rev. B **102**, 060501(R) (2020).

[12] K. Bouadim, Y. L. Loh, M. Randeria, and N. Trivedi, Single- and two-particle energy gaps across the disorder-driven superconductor–insulator transition, Nat. Phys. **7**, 884 (2011).

[13] G. Lemarié, A. Kamlapure, D. Bucheli, L. Benfatto, J. Lorenzana, G. Seibold, S. C. Ganguli, P. Raychaudhuri, and C. Castellani, Universal scaling of the order-parameter distribution in strongly disordered superconductors, Phys. Rev. B **87**, 184509 (2013).

[14] S. Dutta, J. Jesudasan, and P. Raychaudhuri, Magnetic field induced transition from a vortex liquid to bose metal in ultrathin α-MoGe thin film, Phys. Rev. B **105**, L140503 (2022).

[15] C. Carbillet, S. Caprara, M. Grilli, C. Brun, T. Cren, F. Debontridder, B. Vignolle, W. Tabis, D. Demaille, L. Largeau, K. Ilin, M. Siegel, D. Roditchev, and B. Leridon, Confinement of superconducting fluctuations due to emergent electronic inhomogeneities, Phys. Rev. B **93**, 144509 (2016).

[16] C. Carbillet, V. Cherkez, M. A. Skvortsov, M. V. Feigel'man, F. Debontridder, L. B. Ioffe, V. S. Stolyarov, K. Ilin, M. Siegel, D. Roditchev, T. Cren, and C. Brun, Spectroscopic evidence for strong correlations between local superconducting gap and local altshuler-aronov density of states suppression in ultrathin NbN films, Phys. Rev. B **102**, 024504 (2020).

[17] J. M. Valles, R. C. Dynes, and J. P. Garno, Electron tunneling determination of the order-parameter amplitude at the superconductor-insulator transition in 2D, Phys. Rev. Lett. **69**, 3567 (1992).

[18] S. Y. Hsu, J. A. Chervenak, and J. M. Valles, Magnetic field enhanced order parameter amplitude fluctuations in ultrathin films near the superconductor-insulator transition, Phys. Rev. Lett. **75**, 132 (1995).

[19] P. Szabó, T. Samuely, V. Hašková, J. Kačmarčík, M. Žemlička, M. Grajcar, J. G. Rodrigo, and P. Samuely, Fermionic scenario for the destruction of superconductivity in ultrathin MoC films evidenced by STM measurements, Phys. Rev. B **93**, 014505 (2016).

[20] M. Žemlička, M. Kopčík, P. Szabó, T. Samuely, J. Kačmarčík, P. Neilinger, M. Grajcar, and P. Samuely, Zeeman-driven superconductor-insulator transition in strongly disordered MoC films: Scanning tunneling microscopy and transport studies in a transverse magnetic field, Phys. Rev. B **102**, 180508(R) (2020).

[21] K. Inumaru, K. Baba, and S. Yamanaka, Structural distortion and suppression of superconductivity in stoichiometric B1-MoN epitaxial thin films, Phys. Rev. B **73**, 052504 (2006).

[22] B. T. Matthias and J. K. Hulm, A search for new superconducting compounds, Phys. Rev. **87**, 799 (1952).

[23] G. Hägg, Röntgenuntersuchungen Über Molybdän- Und Wol-framnitride, Z. Phys. Chem. **7**, 339 (1930).

[24] T. Tsuneoka, K. Makise, S. Maeda, B. Shinozaki, and F. Ichikawa, Localization and pair breaking parameter in super-conducting molybdenum nitride thin films, J. Phys.: Condens. Matter **29**, 015701 (2016).

[25] H. Ihara, Y. Kimura, K. Senzaki, H. Kezuka, and M. Hirabayashi, Electronic structures of B1 MoN, Fcc Mo_2N, and hexagonal MoN, Phys. Rev. B **31**, 3177 (1985).

[26] M. Kozejova, V. Latyshev, V. Kavecansky, H. You, S. Vorobiov, A. Kovalcikova, and V. Komanicky, Evaluation of hydrogen evolution reaction activity of molybdenum nitride thin films on their nitrogen content, Electrochim. Acta **315**, 9 (2019).

[27] See Supplemental Material at http://link.aps.org/supplemental/10.1103/PhysRevB.108.184511 for an analysis of the trans-port measurements and B-T phase diagrams and supporting figures for the STM measurement results shown in Figs. 2 and 3.

[28] R. C. Dynes, V. Narayanamurti, and J. P. Garno, Direct measurement of quasiparticle-lifetime broadening in a strong-coupled superconductor, Phys. Rev. Lett. **41**, 1509 (1978).

[29] F. Herman and R. Hlubina, Microscopic interpretation of the dynes formula for the tunneling density of states, Phys. Rev. B **94**, 144508 (2016).

[30] B. L. Altshuler, A. G. Aronov, and P. A. Lee, Interaction effects in disordered fermi systems in two dimensions, Phys. Rev. Lett. **44**, 1288 (1980).

[31] B. L. Altshuler and A. G. Aronov, in *Electron-Electron Inter-actions in Disordered Systems*, edited by A. L. Efros, and M. Pollak, Modern Problems in Condensed Matter Sciences Vol. 10 (Elsevier Science/North-Holland, New York, 1985), p. 1.

[32] J. M. Graybeal and M. R. Beasley, Localization and inter-action effects in ultrathin amorphous superconducting films, Phys. Rev. B **29**, 4167 (1984).

[33] M. Kuzmiak, M. Kopčík, F. Košuth, V. Vaňo, P. Szabó, V. Latyshev, V. Komanický, and P. Samuely, Suppressed super-conductivity in ultrathin Mo_2N films due to pair-breaking at the interface, J. Supercond. Nov. Magn. **35**, 1775 (2022).

[34] V. Hašková, M. Kopčík, P. Szabó, T. Samuely, J. Kačmarčík, O. Onufriienko, M. Žemlička, P. Neilinger, M. Grajcar, and P. Samuely, On the origin of In-Gap states in homogeneously disordered ultrathin films. MoC case, Appl. Surf. Sci. **461**, 143 (2018).

[35] A. M. Clogston, Upper limit for the critical field in hard super-conductors, Phys. Rev. Lett. **9**, 266 (1962).

[36] S. Bogdanovich, P. Dai, M. P. Sarachik, and V. Dobrosavljevic, Universal scaling of the magnetoconductance of metallic Si:B, Phys. Rev. Lett. **74**, 2543 (1995).